Separation and Purification Technology 298 (2022) 121613

Contents lists available at ScienceDirect

Separation and Purification Technology

journal homepage: www.elsevier.com/locate/seppur

Enhanced boron modified graphitic carbon nitride for the selective photocatalytic production of benzaldehyde

M. Alejandra Quintana, Rafael R. Solís *, M. Ángeles Martín-Lara, Gabriel Blázquez, F. Mónica Calero, Mario J. Muñoz-Batista *

Department of Chemical Engineering, University of Granada, 18074 Granada, Spain

ARTICLE INFO

Keywords:
Graphitic carbon nitride
Boron
Benzaldehyde
Photocatalysis

ABSTRACT

Graphitic carbon nitride is a non-metal photocatalyst easily prepared from nitrogen organic compounds through green synthesis processes that do not require the use of solvents. This work proposes the use of boron to modify the layered g-C_3N_4 structure by incorporating B to induce defects aimed at the enhancement of the photocatalytic activity. Boron-modified graphitic carbon has been obtained using elemental B and $NaBH_4$ as precursors. The XRD and FTIR characterization results suggest that the C and N positions of g-C_3N_4 can be replaced by B, resulting in a layered modified structure in which the tri-s-triazine units are altered. The exchange of B atoms differed from the boron precursor according to the analysis of the chemical properties of the surface. Thus, the elemental B had a preference to exchange positions with N atoms, whereas the use of $NaBH_4$ led to the substitution of B into the C positions. This difference considerably affected the photocatalytic activity during the selective oxidation of benzyl alcohol. The sample modified with $NaBH_4$ led to the highest oxidation rate and selectivity linked to a lesser recombination effect than the other samples according to photoluminescence tests. This work provides evidence about the convenience of the selection of precursors during the modification of g-C_3N_4. The photon absorbance rate was determined for the estimation of the quantum yield. Although the photon absorbance rate was quite similar in all the cases, the different registered kinetics led to a maximum quantum efficiency of 0.15% for NaBCN.

1. Introduction

Graphitic carbon nitride (g-C_3N_4) is a novel metal-free and non-toxic photocatalyst with promising optoelectronic properties in a wide range of photocatalytic applications [1]. It displays bandgap energy ca. 2.7 eV which allows better harvesting of the solar spectrum if compared to traditional TiO_2 [2]. g-C_3N_4 represents an environmentally friendly alternative since it is based on carbon, nitrogen, and hydrogen and can be easily prepared from nitrogen natural organic compounds such as melamine, urea, or cyanamide, among others [3,4]. The synthesis can be achieved by calcination under inert atmosphere or by hydrothermal treatment under pressure [5]. Analogously to graphene, pristine g-C_3N_4 is a polymeric monolayer of coupled tri-s-triazine (C_6N_7) rings connected by planar amino groups that can be tunable into different morphologies including nanosheets, nanotubes, or quantum dots [6]. Since it was first applied for water splitting [7], numerous applications have been proposed for diverse photocatalytic scenarios, including energy production [8], CO_2 conversion [9], organic transformations [10], water treatment [11], disinfection [3,12] or as sensor [6].

Several modifications have been proposed to enhance the activity of g-C_3N_4 [13]. Some examples of this improved photoactivity include the modification of the pristine structure aimed at the formation of nitrogen vacancies [14], modification of the layered structure with non-metal [15-18] and metal doping [16], the deposition of noble metal nanoparticles [19], anchoring of Na [20], the formation of hetero-structures based in photocatalytic metal oxides [2,15], Mxenes [21] or other organic semiconductors such as Metal Organic Frameworks [22]. Non-metal doping is an environmentally friendly alternative since it does not consider the use of expensive metals that could raise problems of metal leaching during photocatalytic performance. Diverse non-metal options are reported in the literature pursuing improved visible light absorption, increased carrier mobility, production of more active sites, and reduction of the recombination rate of photo-generated charges. The simplest modification of g-C_3N_4 includes the partial oxygenation of

* Corresponding author.
E-mail addresses: rafarsolis@ugr.es (R.R. Solís), mariomunoz@ugr.es (M.J. Muñoz-Batista).

https://doi.org/10.1016/j.seppur.2022.121613
Received 21 April 2022; Received in revised form 22 June 2022; Accepted 26 June 2022
Available online 30 June 2022
1383-5866/© 2022 The Author(s). Published by Elsevier B.V. This is an open access article under the CC BY-NC-ND license (http://creativecommons.org/licenses/by-nc-nd/4.0/).

the g-C_3N_4 structure [23]; however, other non-metal atoms have been successfully incorporated into the structure such as boron [24-27], phosphorous [28], sulfur [29], or halides [30,31]. Boron is an interesting alternative to modify the g-C_3N_4 structure due to the similar chemical properties of boron, carbon, and nitrogen which have raised the attention for a large range of applications owing to their outstanding features [32]. Boron can be exchanged by either carbon or nitrogen positions [33], leading to very interesting photoelectronic properties and defects in the structure.

The selective oxidation of alcohols is one of the most relevant and established transformations into added-value chemicals, i.e. aldehydes and ketones, in industrial catalysis. Currently, diverse technologies are already implemented such as thermo-catalysis, catalysis, and electro-catalysis [34-36]. Among them, photocatalysis is an emerging alternative that can help the migration of traditional technologies to other more respectful with the environment either due to their milder working conditions, the cost-efficient energy input compared to the traditional thermo-catalysis, or the reduction of consumed solvents [37].

This work reports the use of boron-modified graphitic carbon nitride as a novel metal-free photocatalyst for the selective oxidation of benzyl alcohol to the added-value benzaldehyde. Although g-C_3N_4 modified with boron has been reported using $NaBH_4$ in solid stated process for the photocatalytic production of O_2 [24] or H_2 [25], there is no information of the comparison efficiency with other precursors such as elemental boron. Moreover, these materials have not been tested in the photocatalytic production of aldehydes with industrial interest. For that reason, this work is focused on the use and comparison of two different boron precursors have been selected, elemental boron and sodium borohydride to generate defects that enhance the activity and selectivity toward the production of benzaldehyde from benzyl alcohol. A complete characterization including N_2 physisorption, XRD, XPS, FTIR, DRS UV–visible, and photoluminescence technique was applied to unveil the connection between the boron modified g-C_3N_4 and the photocatalytic activity observed. The use of $NaBH_4$ as the precursor, which promotes the exchange of B into carbon positions, led to the best results either reaction rate or selectivity. The photoelectronic characterization results suggested that, compared to the bare g-C_3N_4, the bandgap was reduced (from 2.72 to 2.28 eV) and the recombination effect was considerably weakened. The selection of the suitable B precursor strongly impacts not only the structural changes but also the photoactivity response.

2. Experimental

2.1. Materials and catalysts synthesis

Analytical grade benzyl alcohol (>99%) and benzaldehyde (>99%) standards were used as received. HPLC grade acetonitrile and methanol were used for analytical purposes. Ultrapure water (18.2 MΩ·cm) from a Direct-Q®-UV system (Millipore®) was used in all the solutions preparation.

The graphitic carbon nitride (g-C_3N_4, CN) was prepared as previously reported in the literature from the pyrolyzation of melamine during 2 h at 550 °C with a heating rate of 9 °C·min^{-1} [27]. Next, the yellowish CN was washed with water and the higher particles were discharged by decantation. The suspended CN particles were filtered and dried at 80 °C. The boron modified samples were prepared via calcination under an N_2 inert atmosphere [24]. Briefly, 1.0 g of CN and 0.4 g of $NaBH_4$ (>99%, Sigma-Aldrich®), were mixed and grounded in a mortar. The sample modified with elemental boron (>95%, Sigma-Aldrich®) was added as the equivalent B amount in the 0.5 g of $NaBH_4$. The mixed powder was calcined at 450 °C for 1 h with a ramp of 10 °C·min^{-1} with a gas flow rate of 20 mL N_2·min^{-1}. After cooling to room temperature, the resulting brownish samples were washed several times with water and dried at 80 °C overnight. The boron modified CN with elemental boron was labeled as BCN whereas if $NaBH_4$ was used as the precursor, the sample was named NaBCN. Preliminary tests were carried out in a thermogravimetric balance to ensure the thermal stability of the samples at the selected temperature. Only a 4% mass loss was recorded.

2.2. Characterization of the solids

The thermal stability of the samples was evaluated in a Perkin Elmer (model STA 6000) thermobalance. A constant heating rate of 10 °C·min^{-1} was used under N_2 atmosphere (flow rate, 20 mL/min) from room temperature to 450 °C. The crystalline structure was studied by X-Ray Diffraction (XRD) in a Bruker D8 Discover diffractometer w using a Cu Kα radiation source (λ = 1.5406 Å) and a Pilatus3R 100 K-A detector within a 2θ range of 8-80° at a rate of 0.08°·min^{-1}. The software *Match!* ® and the Crystal Open Database (COD) library were used to process the diffractograms obtained. The stretching of the bonds in the structure was studied by Fourier Transform InfraRed (FTIR) analysis, carried out in a Perkin-Elmer device (model Spectrum65) within 400–4000 cm^{-1}. The chemical composition of the surface was analyzed by X-ray Photoelectron Spectroscopy (XPS) in a Kratos AXIS UltraDLD device working with an X-ray source from Al Kα. The XPS spectra were referenced to the C1s peak of adventitious carbon to 284.6 eV. The software *XPSpeak 4.1*® was used for the deconvolution of the peaks, considering a Shirley background correction. Scan Transmission Electron Microscopy (STEM) was used to study the morphology and the distribution of element composition with High-Angle Annular Dark Field (HAADF) detection and Electron Disperse X-Ray (EDX) analysis in a Thermo Fisher Scientific TALOS F200X device. The elemental composition, i.e. C, N and H, was analyzed in a Thermo Scientific™, Flash 2000 analyzer. The textural properties (surface area and pore volume) were determined from N_2 adsorption–desorption at 77 K performed in an ASAP 2020 equipment (Micromeritics). The specific surface area was obtained by the Brunauer-Emmett-Teller method (S_{BET}). The optical properties were obtained by Diffuse Reflectance Spectroscopy (DRS) in the UV–visible range in a Varian Cary 5E spectrophotometer. From the reflectance spectrum and the application of Tauc plot method [38], the bandgap values were estimated. The recombination rate of the photogenerated electrons was assessed by photoluminescence (PL) analysis in a Varian Cary Eclipse device under an excitation wavelength of 365 nm.

2.3. Photocatalytic production of benzaldehyde

Photocatalytic reactions were carried out in a discontinuous type annular photoreactor, see scheme in Fig. 1, with the liquid mixture circulating through the jacked space and radiation source (Sylvania® F11W T5 BL368 lamp, emitting at 365 nm, 11 W) located in the center. To keep the temperature constant to 20 °C, the mixture was recirculated to a stirring tank equipped with a jacketing system. Excess air was bubbled in this stirring tank to maintain an oxidizing environment which has been reported as beneficial for this reaction [39]. Every 30 min during 4 h of reaction, samples were extracted, and the photocatalyst was removed by centrifugation. Previous to irradiation, a 30 min adsorption step was carried out. Experiments were carried out by triplicate and the relative standard deviation error was minor to 5%. The importance of photo-generated and radical species was assessed with scavenging experiments in the presence of methanol (10 mM), oxalic acid (10 mM) or N_2 bubbling following the same described procedure.

The radiation intensity of the lamp was quantified by an in-situ chemical actinometry based on the photoreduction of the ferrioxalate combined with a polyoxometalate ($Na_2SiW_{12}O_6$) to monitor the temporal depletion of the ferrioxalate complex [40]. The experimental conditions included oxalic acid 60 mM, $FeCl_3$ 5 mM, and $SiW_{12}O_{40}^{4-}$ 1 mM. The pH was adjusted to 4.5 with HCl and NaOH to prevent self-decomposition of the polyoxometalate complex. Considering a quantum yield $\phi = 0.18$ mol·$Einstein^{-1}$ [40] at 365 ± 10 nm during the photoproduction of $SiW_{12}O_{40}^{5-}$, the radiation intensity value obtained was $I_0 = (2.2 \pm 0.1)\cdot10^{-4}$ Einstein L^{-1} min^{-1}.

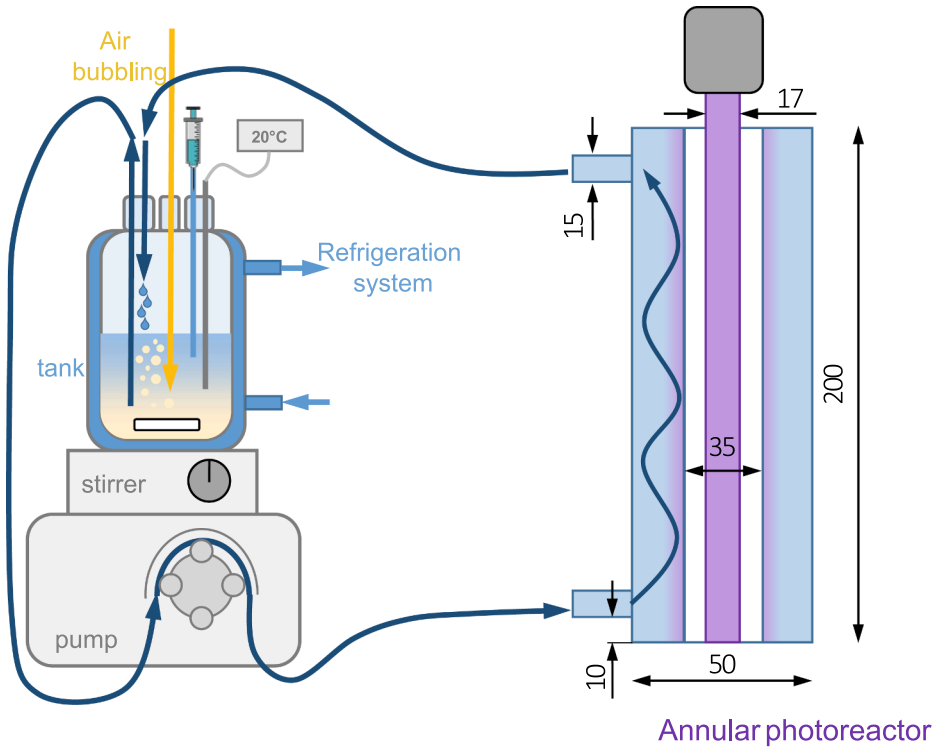

Fig. 1. Experimental setup of the photoreaction system (dimensions expressed in mm). *Experimental conditions:* $V_{photorreactor} = 200$ *mL;* $V_{tank} = 150$ *mL;* $T = 20$ *°C.*

The concentration of benzyl alcohol (BA) and benzaldehyde (BD) during the photoreaction was quantified by High-Performance Liquid Chromatography (HPLC) technique in a Shimadzu LC-10 device coupled to DAD UV–visible detection. The stationary phase was a Kromasil C18 column 100 5C18 (100 Å, 5 µm, 2.1 × 150 mm) and the mobile phase consisted of a constant elution of a mixture of methanol (2.5%), acetonitrile (27.5%), and 0.1% H_3PO_4 ultrapure water (70%) pumped at 1.0 mL min^{-1}. The BA (retention time, 3.7 min) was quantified at 215 nm and the BD (retention time, 6.4 min) at 248 nm. The limit of detection [41] was calculated as, respectively, 26 and 14 µM for BA and BD. The Total Organic Carbon (TOC) was analyzed in a Shimadzu® TOC-V_{CSH} analyzer.

The quantum efficiency (Q_E) was calculated according to the Eq. (1), following the IUPAC recommendations [42-44], which defines the Q_E as the ratio of the number of molecules reacting, i.e. the reaction rate, by the number of photon which interact with the catalyst, i.e. the photon absorption rate [45]:

$$Q_E(\%) = \frac{r_{BA_0}\ (\text{molÂ·m}^{-3}\text{Â·s}^{-1})}{e^{a,v}\ (\text{EinsteinÂ·m}^{-3}\text{Â·s}^{-1})}\text{Â·100} \quad (1)$$

The initial BA degradation rate ($r_{BA,0}$) was determined from the slope of the temporal evolution of the C_{BA} extrapolating at the initial time, or after the reaction started in case of appreciating an inactivation period.

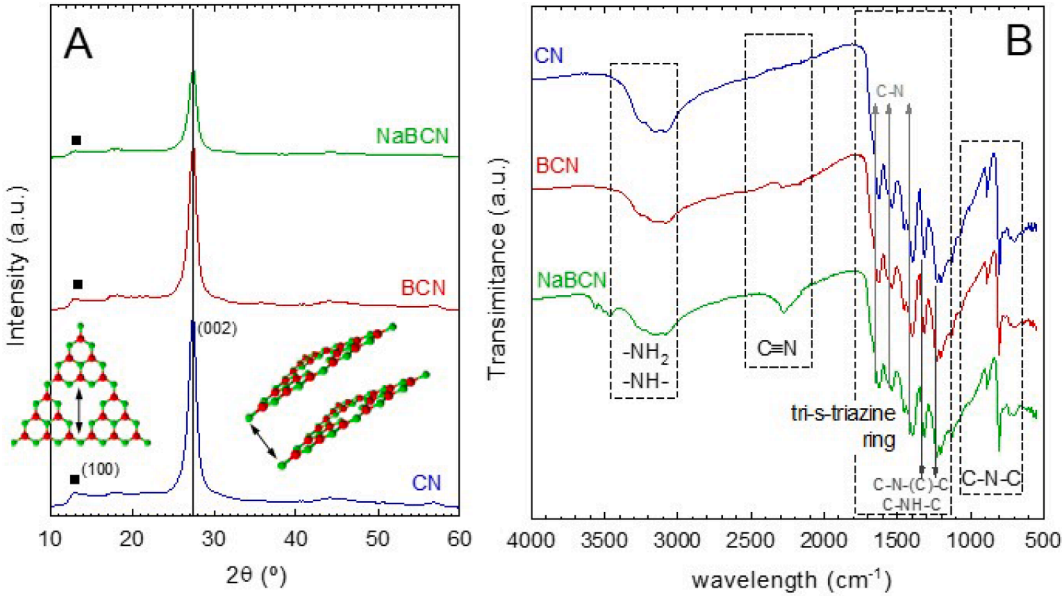

Fig. 2. Changes in the XRD pattern (A) and FTIR spectra (B) of CN after B incorporation.

To determine the photon absorption rate ($e^{a,\nu}$), the radiative transfer equation (RTE) was solved for the used reactor which needs as first step the determination of the optical properties of the catalytic suspensions. Detailed description of the mathematical procedure for both optical properties and photon rate estimations are provided in the supporting information.

3. Results and discussion

3.1. Characterization of the boron modified g-C_3N_4

The XRD technique was used to assess the changes in the graphitic carbon structure of CN after the incorporation of boron. Fig. 2A illustrates the registered XRD patterns for the CN, BCN, and NaBCN samples. As shown in this figure, the pristine sample, CN, presents two characteristic peaks reported in g-C_3N_4 samples, one located at $2\theta = 13.4^\circ$, whose intensity is almost negligible, and a second intense peak at 27.3° which are assigned, respectively, to the (1 0 0) and (0 0 2) planes [24]. The (1 0 0) plane refers to the in-plane of tri-s-triazine units that build the g-C_3N_4 sheet while the (0 0 2) plane, the most important and intense, results from the presence of interconnected layers. The almost negligible (1 0 0) peak in the CN sample suggests a lack of organized triazine units inside the sheet; nonetheless, the presence of an intense peak at 27.3° corroborates the formation of the layered structure. The incorporation of boron as elemental B led to a decrease of the (0 0 2) plane in the BCN sample, due to the increase of the disorder in the structure. The addition of $NaBH_4$ instead of elemental B contributed to the higher destruction of the interlayered structure giving to a lower peak.

Fig. 2B depicts the FTIR spectra of CN, BCN, and NaBCN samples. There is a wide band within 3000–3500 cm^{-1} related to the vibration –NH_2 and –NH– groups. The incorporation of boron with the two precursors, elemental B, and $NaBH_4$, led to a slight depletion of this band as shown for BCN and NaBCN spectra. The CN sample also presents a peak located at ~ 810 cm^{-1} which is attributed to o the out-of-plane bonding vibration characteristics of triazine [24]. A decrease of this peak is observed after the incorporation of B with NaBCN. Moreover, a group of peaks between 900 and 1800 cm^{-1} is originated due to the stretching of the aromatic C-N heterocycles [24]. Concretely, the intense peaks at 1620, 1530, and 1390 cm^{-1} can be assigned to the aromatic C-N stretching vibration [46,47]. The bands at 1310 and 1230 cm^{-1} correspond to the stretching vibration of C-N-(C)-C or C-NH-C bonds [46,47]. This group of peaks suffered soft modifications during the incorporation of boron, being the sample NaBCN the one giving less intensity for these peaks. A new peak at 2270 cm^{-1} emerged in the sample NaBCN. This peak corresponds to the asymmetric stretching vibration of the C≡N group that appears as a consequence of a thermal reaction between elemental B or $NaBH_4$ and g-C_3N_4 [24,25]. The presence of this C≡N group introduces nitrogen defects into the g-C_3N_4 structure. This peak appears in both boron-modified samples; however, the intensity acquired is higher in the NaBCN sample if compared to BCN. Summarizing, not great changes in FTIR footprint were appreciated rather the alteration on nitrogen defects. For that reason, a more sensitive superficial technique such as XPS was carried out.

The textural properties were assessed by N_2-physisorption analysis, see results in Table 1. The N_2 uptake isotherms are available in Fig. S1. The samples were macroporous with low specific surface area. The S_{BET} values slightly decreased with the boron incorporation, being the $NaBH_4$ the precursor that produced a greater modification.

The chemical changes on the surface of the samples after boron modification were studied by the XPS technique. Fig. 3 provides a detailed analysis of the high-resolution C1s, N1s, and B1s regions. As observed, the incorporation of boron in the structure partially modifies the original C1s and N1s spectra of the bare graphitic carbon nitride structure. It should be noted that as the B content was minor, the modifications displayed are a plausible suggestion of the bond changes. Moreover, an intense peak of B1s was registered in BCN and NaBCN samples, which proves the presence of boron after the synthesis. The spectra were deconvoluted according to the expected contributions reported in the literature. The N1s peak of CN can be explained as the sum of three contributions related to C_3–N (N_{3C}, 399.9 eV), N–C = N (N_{2C}, 398.4 eV), and N–H_x (401.0 eV) bonds [25-27,48]. The peak N_{3C}, considerably diminished in intensity, which provides evidence of a B attack to these points of s-triazine structure. Also, the peak related to -NH_x terminal defects decreased after B incorporation, suggesting the susceptibility to be attacked. As a consequence of the incorporation of boron in the structure, two extra contributions, B = N-C (399.0 eV) and N-(C_2)B (400.4 eV) appeared in the N1s network [27], which suggest the integration of B in the graphitic structure. The C1s region displayed major changes. The C1s peak of graphitic carbon nitride is commonly deconvoluted in sp^2 N = C-N (287.9 eV), sp^3 C-C/C-N (285.2 eV), and sp^2 C-C/C = C (284.4 eV) bonds [25]. The modification of the CN sample with boron intensively modified the carbon network. As the result of the formation of defects due to the boron presence, the contribution of the sp^2 N = C-N peak decreases, the contribution of sp^2 C-C/C-N defects raised, and the sp^2 C-C/C = C decreased in the NaBCN sample. The N/C ratios were, according to XPS analysis, highly modified being 0.94 (CN) > 0.55 (BCN) > 0.49 (NaBCN). The modification with boron led to a decrease of the N/C ratio, confirmed also elemental analysis technique (Table 1). In the case of elemental analysis, although the values are different due to the superficial character of XPS technique, the decrease tendency after the modification with boron was the similar and closer to the theoretical expected N/C = 4/3 value of g-C_3N_4. This difference between techniques provides evidence of the incorporation of boron just at a surface level. According to the atomic percentages of elements in the surface, the pristine CN sample displays a very low amount of O. The two contributions detected in O1s peak were terminal –OH and C = O groups [49] (**Fig. S2**). The global O percentage raises in the order NaBCN > BCN > CN probably also promoted by the oxidation of boron after contact with water in the washing steps. From the results, it can be deduced that boron alters the structure of bare CN not only by exchanging positions in the structure but also by generating terminal oxygenated defects. The modification with boron using elemental boron or $NaBH_4$ as precursors led to very different B1s profiles. Due to the lower level of boron respect to the other elements, B1s spectrum can be used to deduce the boron bonding state in the structures. Up to four different contributions were identified, i.e. elemental boron (186.8 eV), NC_2-B (188.1), B-N (190.3 eV), and B related to oxides or hydroxides (191.9 eV) [27,50,51]. If elemental B was the precursor, the incorporation of B in the structure was placed as N-(C_2)B. Nonetheless, if $NaBH_4$ was used, the incorporation of boron as BN peak is predominant and the

Table 1
Characterization of the CN, BCN, and NaBCN samples.

Sample	S_{BET} ($m^2\ g^{-1}$)	Surface atomic percentage (%) by XPS				Atomic N/C ratio		Bandgap (eV)
		C	N	O	B	XPS	Elemental analysis	
CN	13.0	49.4	46.7	3.9	–	0.94	1.54	2.72
BCN	11.5	51.3	28.3	9.4	11.0	0.55	1.50	2.53
NaBCN	3.7	38.9	19.0	21.5	10.2	0.49	1.31	2.28

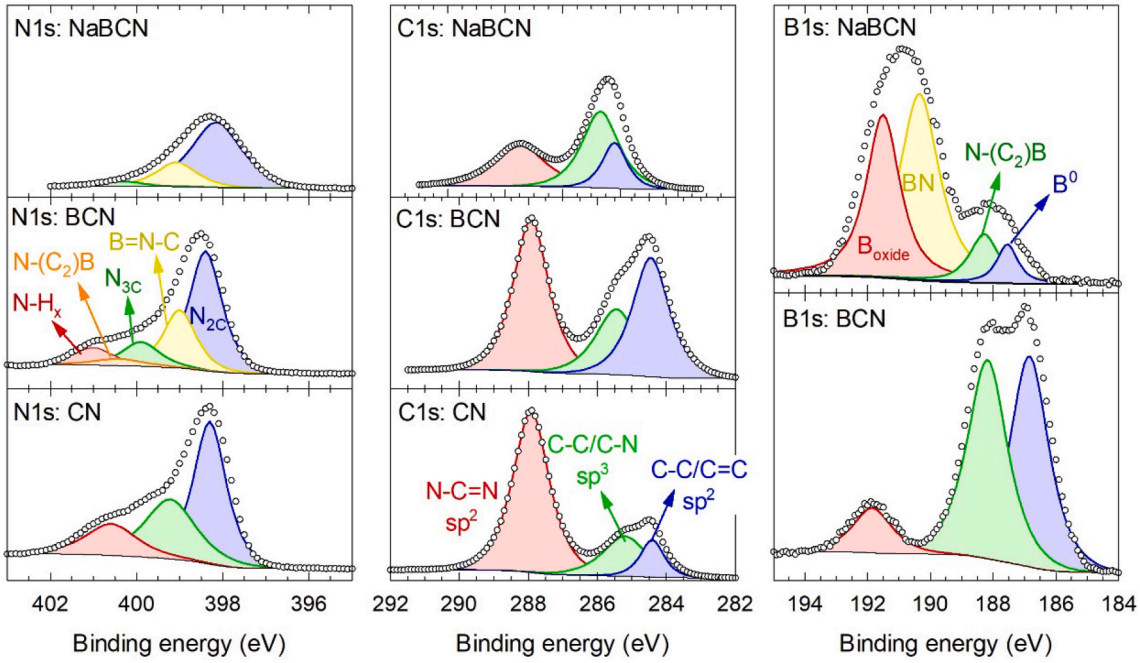

Fig. 3. Changes in XPS spectra of N1s (left), C1s (center), and B1s (right) of CN after B incorporation.

N-(C_2)B peak was minor. These results suggest that the nature of the B precursor could direct the positions in which B is going to be incorporated, which means elemental B prefer to attack C atoms while if $NaBH_4$ is used B is replaced in the N positions. Other secondary chemical states of B not meaning an exchange of this element into N or C positions of CN were also detected, i.e. elemental boron in BCN and boron oxide in NaBCN. The major presence of boron oxide in B1s spectrum would also contribute to explain the major content of oxygen in NaBCN sample. The XPS surface atomic composition is available in Table 1. Both boron modified samples, BCN and NaBCN presented very similar B incorporation yields in their structures, 11.0 and 10.2% respectively.

The morphology and element distribution of NaBCN sample was analyzed by STEM and EDX mapping. The Fig. 4 shows an example of the pictures obtained. The morphology displayed as layered flakes and the EDX mapping confirmed the presence of B, C and N. As observed in the individual mapping, B was uniformly distributed around the flake

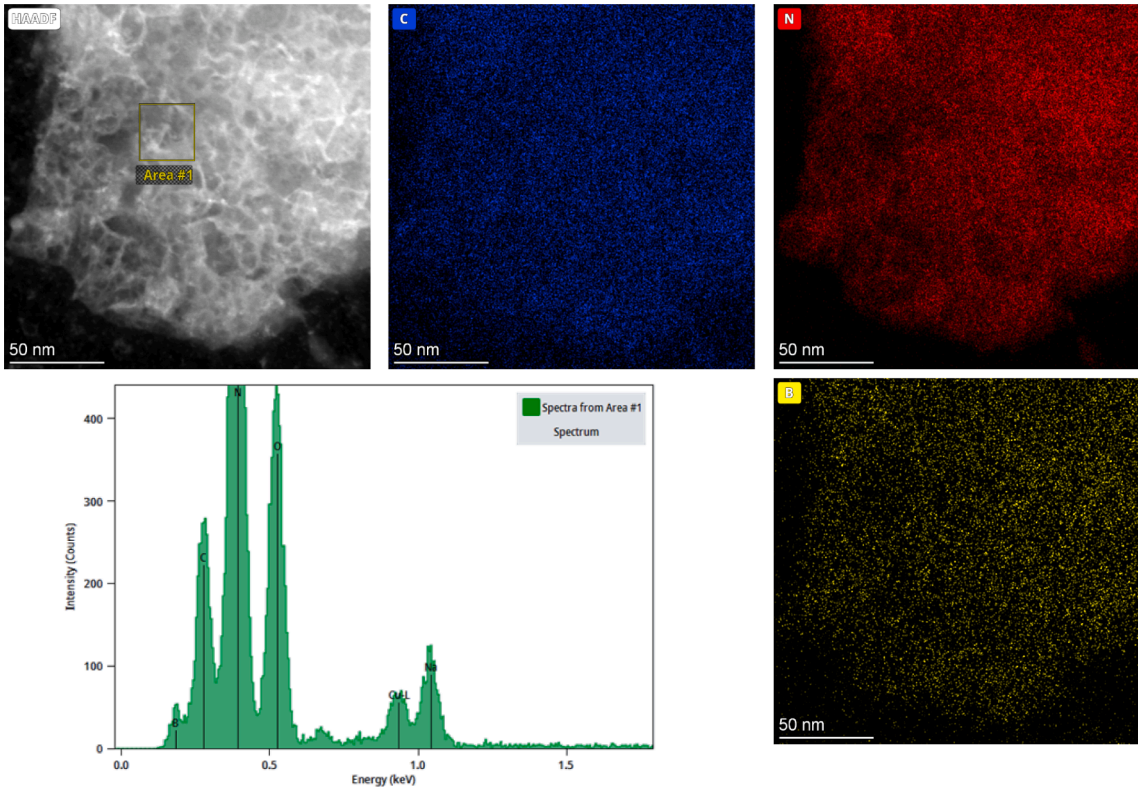

Fig. 4. STEM image and EDX mapping of NaBCN sample.

particle.

Fig. 5A displays the UV–visible absorption spectra of the samples. As boron was incorporated in the structure, the edge of CN was red-shifted. The calculated bandgaps values, see Fig. 5B and Table 1, decreased from 2.72 eV in CN to 2.58 eV in BCN and 2.53 eV in NaBCN. Thus, the incorporation of boron in the structure of CN broadened the light absorption range by decreasing the bandgap value. Therefore, the boron-modified materials are expected to better harvest visible radiation; however, due to the monochromatic nature of the lamp used in the photo-reactor, the materials will only take advantage of the band gap reduction rather than the widening of the radiation absorptivity.

Despite the fact of the differences register in the optical properties, the incorporation of boron in the structure seems not to have a significant influence in terms of the photon absorption rate. The boron-modified samples displayed similar behavior due to the net light emitted by the used UV lamp. In agreement with the UV–visible spectra, the increase of the light absorption level of the visible range was also detected when the properties of the catalytic suspension were determined. As depicted in Figure S3, the profiles of the related optical coefficients, i.e. the spectral absorption coefficient, the spectral scattering coefficient, and the scattering phase, show some differences. Nonetheless, these dissimilarities do not translate, as could be expected, into a significant modification of the rate of UV light photons absorbed by the materials, as presented in Fig. 6. As discussed later, the modification of the catalytic properties seems to be associated with an improvement in the load handling processes. This is also supported by the catalytic test under visible irradiation conditions (Sylvania® F6W T5 Daylight lamp, emitting over 420 nm), which shows negligible catalytic activity (data not included) under the same operating condition described in the experimental section.

3.2. Photocatalytic performance for the production of benzyl alcohol

The graphitic carbon nitride and the boron modified samples were used as potential photocatalysts for the selective oxidation of benzyl alcohol to benzaldehyde. Fig. 7A shows the photocatalytic results in terms of initial reaction rates and selectivity towards benzaldehyde production. The normalized temporal evolution of BA and BD concentration are available in Fig. S6. A preliminary test under irradiation and without photocatalyst proved the negligible contribution of photolysis of BA. Adsorption of BA onto the samples was also discharged by carrying out 30 min of previous adsorption test before switching the lamp on. The BA conversion of the samples after 4 h, see Fig. S6, followed the order NaBCN (29 %), BCN (15 %) > CN (13 %). A pseudo-first order kinetics was registered except for the NaBCN sample which performed an initial inhibition step. The initial rate of benzyl alcohol removal

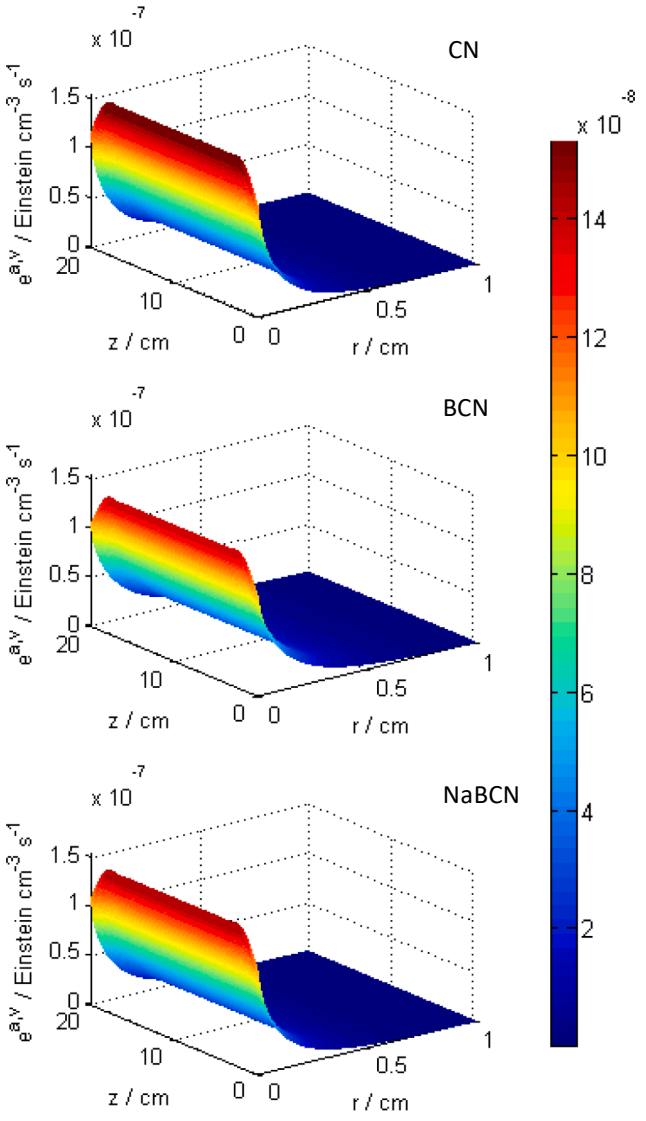

Fig. 6. Local volumetric rate of photon absorption of CN, BNC and NaBCN.

($r_{BA,0}$) did not significantly change if elemental boron was used as a modifier. Nevertheless, in terms of benzaldehyde production rate, the sample BCN performed a ~ 3-folded $r_{BD,0}$ value and therefore, an

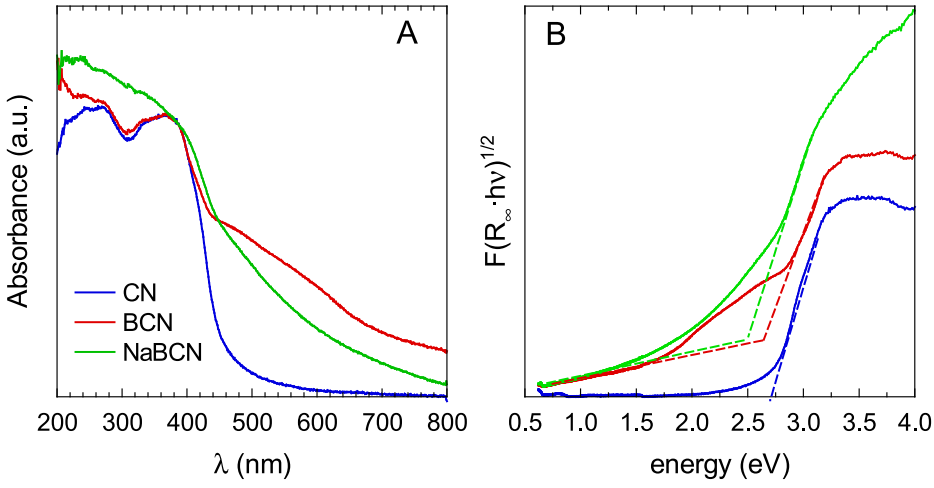

Fig. 5. Changes in DRS-UV–visible spectra (A) and bandgap determination by Tauc plot method (B) of CN after B incorporation.

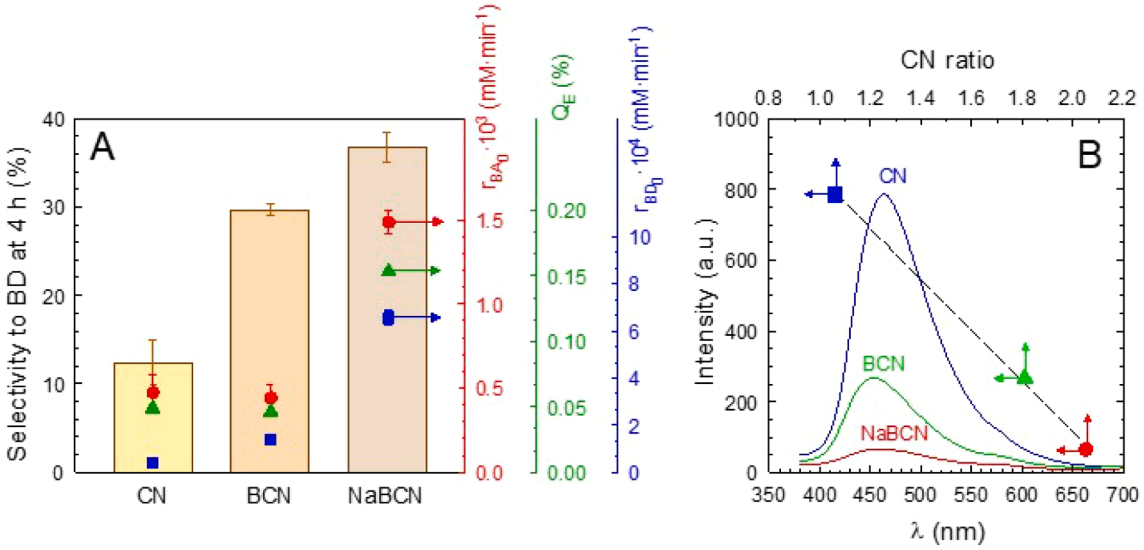

Fig. 7. Changes in the photocatalytic performance in aqueous solution (A), PL spectra (B) of CN after B incorporation, and correlation between maximum PL value and CN ratio (B). *Experimental conditions: V = 350 mL, T = 20 °C, $C_{BA,0}$ = 0.7 mM; C_{CAT} = 0.5 g L^{-1}.*

improved selectivity of BA to BD, i.e. ca. 30% for BCN and 12% for CN. If $NaBH_4$ was used as the boron precursor, enhanced reaction rates were registered. Regarding $r_{BA,0}$, NaBCN displayed a 3 times higher value; while for $r_{BD,0}$ photo-production the value was almost 16 times raised. The selectivity from BA to BD was also improved by a value of 36%. The BA oxidation has been reported to produce not only BD. The further oxidation of the aldehyde generates benzoic acid [52,53]. Moreover, benzyl benzoate has been reported after the reaction between oxidized product benzoic acid and reactant benzyl alcohol [54]. In some studies, certain mineralization degree has been reported [52]; however, it was not the case of this work since no significant changes of TOC were registered. The Q_E values of the BA disappearance were calculated from the rate of photon absorbance rate as described in Eq. (1). The NaBCN sample led to the highest value, Q_E = 0.153%; whereas the CN and BCN displayed very similar results, 0.048 and 0.046%, respectively. These results suggest that the defects created in the CN structure by B incorporation enhanced both the photo-activity and the selectivity of the photocatalysts toward the BD formation. Moreover, the sample NaBCN, in which B exchanges positions with C atoms as suggested by XPS analysis, resulted more reactive leading to higher $r_{BA,0}$ and $r_{BD,0}$ values. These photo-activity results are in good agreement with the recombination extent of the electron-hole pair. The PL technique, whose results are displayed in Fig. 7B, was used to compare the behavior of the three samples by contrasting the intensity of the PL peak which is associated with a higher recombination rate. Hence, the sample CN, which was the most inefficient for BD production, led to the highest PL peak whose maximum was located at ~ 470 nm. The modification of the graphitic carbon nitride structure lead to enhanced solids whose PL peaks considerably decreased in the order CN > BCN > NaBCN. The B incorporation also decreases the wavelength at which their maximum was located, ca. 460 nm. The intensity of the PL peak was correlated to the CN ratio, as shown in Fig. 7B. This figure depicts a linear correlation between both variables, which suggests that the creation of defects in the graphitic carbon nitride reduces the recombination effect, the reason why the photocatalytic activity was increased.

The photocatalytic oxidation of benzyl alcohol to benzaldehyde is frequently carried out in the presence of organic solvents as reaction media instead of the aqueous solution to rise the selectivity of the reaction [39,52]. Among others, acetonitrile is commonly used to ensure a more selective environment of the reaction, decreasing the rate of the formation of powerful oxidants such as $HO^{\bullet}$, leading therefore the reaction toward other more selective reactive species such as $O_2^{\bullet-}$ [55]. Moreover, the beneficial effect of using acetonitrile is related to the larger amount of O_2 dissolved if compared to water [56]. After the light excitation, electrons are generated and migrate to the conduction band of the catalyst and move to the surface of the catalyst where they react with adsorbed O_2 to form $O_2^{\bullet-}$. $O_2^{\bullet-}$ abstracts proton from the BA to form the BD [54]. In the valence band, water molecules, if present, could be oxidized by holes to $HO^{\bullet}$, that may contribute to the further oxidation of BD into other species that can lead complete oxidation to CO_2 [53], which was not observed in this study. Although the selectivity could be compromised, the use of water as the solvent is highly desired from the ecological, economical, and safety points of view. For that reason, some tests were carried out to assess the influence of acetonitrile as solvent at different acetonitrile: water ratios in the most active solid sample, that means NaBCN. The results of the initial reaction rates and the selectivity towards benzaldehyde production are depicted in Fig. 8. The normalized temporal evolution of BA and BD concentration are available in Fig. S7. The addition of acetonitrile negatively impacted the reaction rates, either the degradation of BA or the formation of BD due to the scavenger effect of the organic solvent with hydroxyl radical which promotes further reaction of BD. Despite this effect, the selectivity was considerably raised if 20% of acetonitrile was added, ca. 82%. Higher proportions of ACN resulted detrimental for the selectivity of BA to BD. Although the selectivity is undoubtedly raised with a 20% of ACN, the

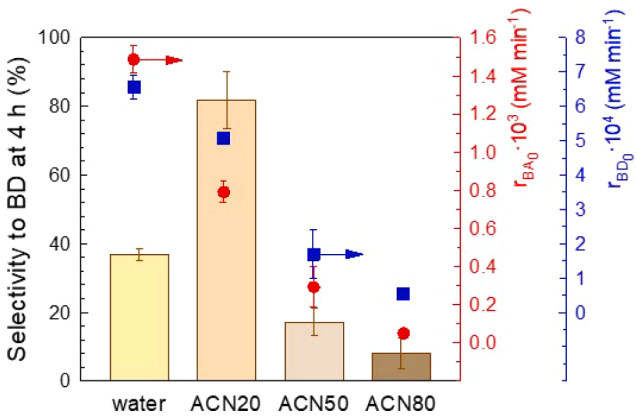

Fig. 8. Influence of acetonitrile (ACN) in the photocatalytic performance of NaBCN. *Experimental conditions: V = 350 mL, T = 20 °C, $C_{BA,0}$ = 0.7 mM; C_{CAT} = 0.5 g L^{-1}.*

use of water can be justified based on a higher reaction rate and greener conditions.

Some tests in aqueous solution were carried out to assess the relative importance of common oxidant species in the photocatalytic process and investigate the role played by superoxide radicals. Methanol was used as a potential scavenger of hydroxyl radicals [57], oxalic acid as a photo-generating hole trapping agent [58], and the impact played by O_2 was evaluated by replacing it with an inert atmosphere by bubbling N_2 [59]. The results are depicted in Fig. 9. The presence of methanol slightly modified the BA profile registered for the blank test; however, better and faster production of BD was monitored, i.e. selectivity of 56% vs 30% of the blank test, suggesting the importance of hydroxyl radical, not high in the degradation rate of BD but negative for the production of BD. The bubbling of N_2 led to a half reduction of BA conversion, denoting the importance of superoxide radicals in the photocatalytic conversion process. More interesting were the results obtained in the presence of oxalic acid which accelerated the degradation of BA, reaching 100% of conversion after 4 h. The profile monitored for BD, in this case, reached a maximum within 60–90 min, although the selectivity was gradually decreasing due to the high BA converted, i.e. 63–23% in this BA maximum production peak. In this case, oxalic acid may act as a hole trapping agent, enhancing the photo-generation of charges which would explain the enhanced BA degradation rate. It has been reported that the photocatalytic decomposition of oxalate might happen simultaneously with the transfer of electrons from this compound to the valence band of the photocatalyst [58].

The stability of the NaBCN sample after being used was studied by analyzing the solid properties during after being used in aqueous solution, (Fig. 10). The XRD and FTIR changes were analyzed and compared to the fresh sample. The FTIR spectrum of reused NaBCN displayed fewer intensity peaks but still provided the footprint characteristic of graphitic carbon nitride structure. The band related to the vibration –NH_2 and –NH– groups which was poorly defined in the boron modified sample due to the presence of boron, was even more diffuse after the reuse. The new peak at 2270 cm^{-1} emerged in the sample NaBCN associated to the C≡N group was still well defined in the reused sample. The peaks corresponding to the tri-s-triazine (heptazine) ring were considerable weakened although still perceptible. The peak attributed to o the out-of-plane bonding vibration characteristics of triazine (~810 cm^{-1}) was well defined but at lesser intensity. Regarding the changes in XRD pattern after the reused, it is observed that definition of the (0 0 2) peak corresponding to the presence of interconnected layers was kept.

4. Conclusions

The modification of graphitic carbon nitride with boron is a powerful strategy for the enhancement of photocatalytic activity. Moreover, the nature of the boron precursor results also in the high relevance of the chemical properties and, therefore, affects the photocatalytic activity of benzyl alcohol oxidation. The characterization results suggest that elemental boron favors the exchange of boron atoms by nitrogen whereas $NaBH_4$ prefers the exchange into carbon positions. Although both boron sources improved the activity of the solid, the use of $NaBH_4$ resulted in the highest oxidation rate of benzyl alcohol and selectivity to benzaldehyde. A direct correlation between the recombination rate and the number of defects in the structure was observed in PL analysis. The use of acetonitrile as solvent was explored to raise the selectivity. This organic decreased the activity of the solid but addressed the reaction to the formation of benzaldehyde. A proportion of 20% of acetonitrile raised the selectivity to over 80% from 39% observed for water. However, higher proportions of acetonitrile resulted in detrimental selectivity, below the value observed for water. This contribution includes a deep analysis of the light-matter interaction from a strict determination of the quantum yield values of the materials. Although the variation of the photon absorption of the samples showed a relatively low influence to compare the catalytic properties, the determination of the quantum efficiency values has tremendous significance for the comparison of the results of this work with future reports of selective oxidation reactions of alcohols as the measured activity is normalized by the light absorbed by the material. Furthermore, the determination of photon absorption paves the way for intrinsic kinetic studies, which may be the basis for scaling-up efficient catalytic systems for this application.

CRediT authorship contribution statement

M. Alejandra Quintana: Investigation, Methodology. **Rafael R. Solís:** Methodology, Supervision, Writing – original draft, Funding acquisition. **M. Ángeles Martín-Lara:** Investigation, Writing – review & editing. **Gabriel Blázquez:** Investigation, Writing – review & editing. **F. Mónica Calero:** Investigation, Resources, Writing – review & editing, Funding acquisition. **Mario J. Muñoz-Batista:** Conceptualization, Formal analysis, Supervision, Writing – review & editing, Funding acquisition.

Declaration of Competing Interest

The authors declare that they have no known competing financial interests or personal relationships that could have appeared to influence the work reported in this paper.

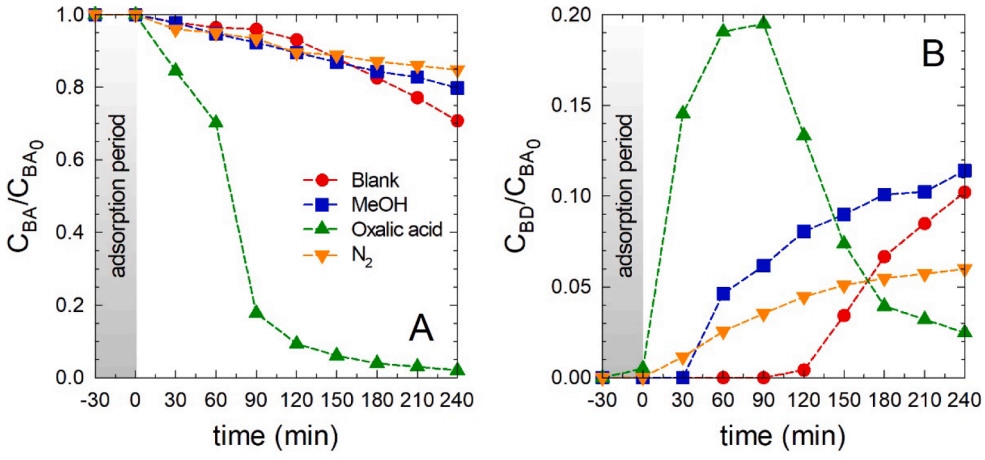

Fig. 9. Time course of benzyl alcohol (A) and benzaldehyde (B) concentrations during the photocatalytic oxidation with NaBCN in the presence of scavengers. *Experimental conditions: V = 350 mL, T = 20 °C, $C_{BA,0}$ = 0.7 mM; C_{CAT} = 0.5 g L^{-1}; $C_{scavenger}$ = 10 mM.*

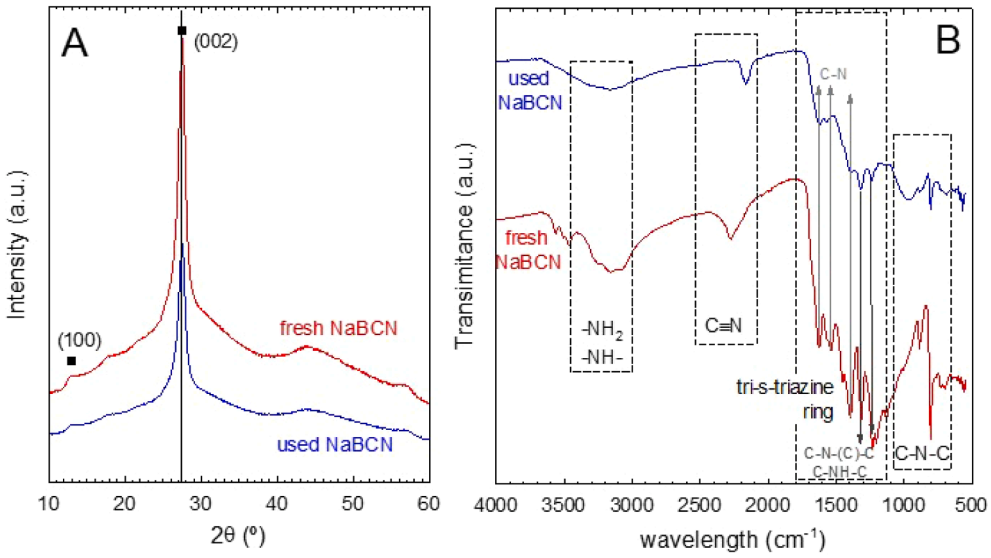

Fig. 10. Changes in the XRD pattern (A) and FTIR spectra (B) of NaBCN after reuse.

Data availability

Data will be made available on request.

Acknowledgements

The authors thank the University of Granada for the "Precompetitive Research Projects for Young Researchers Modality A- Young Doctors" of the 2019 and 2021 UGR Researching Plan (PPJIA2019-09 and PPJIA2021-34 grants). The authors are also grateful to the supporting analyses provided by the external services of the University of Granada (CIC) and the University of Málaga (SCAI). Funding for open access charge: Universidad de Granada / CBUA.

Appendix A. Supplementary material

Supplementary data to this article can be found online at https://doi.org/10.1016/j.seppur.2022.121613.

References

[1] A. Akhundi, A. Badiei, G.M. Ziarani, A. Habibi-Yangjeh, M.J. Muñoz-Batista, R. Luque, Graphitic carbon nitride-based photocatalysts: Toward efficient organic transformation for value-added chemicals production, Mol. Catal. 488 (2020) 110902, https://doi.org/10.1016/j.mcat.2020.110902.

[2] Z. Zhao, Y. Sun, F. Dong, Graphitic carbon nitride based nanocomposites: a review, Nanoscale. 7 (1) (2015) 15–37, https://doi.org/10.1039/C4NR03008G.

[3] C. Zhang, Y. Li, D. Shuai, Y. Shen, W. Xiong, L. Wang, Graphitic carbon nitride (g-C_3N_4)-based photocatalysts for water disinfection and microbial control: A review, Chemosphere. 214 (2019) 462–479, https://doi.org/10.1016/J.CHEMOSPHERE.2018.09.137.

[4] A.A. Yadav, S.-W. Kang, Y.M. Hunge, Photocatalytic degradation of Rhodamine B using graphitic carbon nitride photocatalyst, J. Mater. Sci. Mater. Electron. 32 (11) (2021) 15577–15585.

[5] J. Cheng, Z. Hu, K. Lv, X. Wu, Q. Li, Y. Li, X. Li, J. Sun, Drastic promoting the visible photoreactivity of layered carbon nitride by polymerization of dicyandiamide at high pressure, Appl. Catal. B Environ. 232 (2018) 330–339, https://doi.org/10.1016/J.APCATB.2018.03.066.

[6] M.M. Xavier, P.R. Nair, S. Mathew, Emerging trends in sensors based on carbon nitride materials, Analyst. 144 (5) (2019) 1475–1491, https://doi.org/10.1039/C8AN02110D.

[7] X. Wang, K. Maeda, A. Thomas, K. Takanabe, G. Xin, J.M. Carlsson, K. Domen, M. Antonietti, A metal-free polymeric photocatalyst for hydrogen production from water under visible light, Nat. Mater. 8 (2008) 76–80, https://doi.org/10.1038/nmat2317.

[8] Q. Hao, G. Jia, W. Wei, A. Vinu, Y. Wang, H. Arandiyan, B.-J. Ni, Graphitic carbon nitride with different dimensionalities for energy and environmental applications, Nano Res. 13 (1) (2020) 18–37.

[9] A. Akhundi, A. Habibi-Yangjeh, M. Abitorabi, S. Rahim Pouran, Review on photocatalytic conversion of carbon dioxide to value-added compounds and renewable fuels by graphitic carbon nitride-based photocatalysts, Catal. Rev. 61 (4) (2019) 595–628, https://doi.org/10.1080/01614940.2019.1654224.

[10] B. Long, Z. Ding, X. Wang, Carbon Nitride for the Selective Oxidation of Aromatic Alcohols in Water under Visible Light, ChemSusChem. 6 (11) (2013) 2074–2078.

[11] X. Huo, H. Yi, Y. Fu, Z. An, L. Qin, X. Liu, B. Li, S. Liu, L. Li, M. Zhang, F. Xu, G. Zeng, C. Lai, Porous graphitic carbon nitride nanomaterials for water treatment, Environ. Sci, Nano. 8 (7) (2021) 1835–1862, https://doi.org/10.1039/D1EN00171J.

[12] J. Xu, Z. Wang, Y. Zhu, Enhanced Visible-Light-Driven Photocatalytic Disinfection Performance and Organic Pollutant Degradation Activity of Porous g-C_3N_4 Nanosheets, ACS Appl. Mater. Interfaces. 9 (33) (2017) 27727–27735, https://doi.org/10.1021/acsami.7b07657.

[13] Y. Li, M. Gu, X. Zhang, J. Fan, K. Lv, S.A.C. Carabineiro, F. Dong, 2D g-C_3N_4 for advancement of photo-generated carrier dynamics: Status and challenges, Mater. Today. 41 (2020) 270–303, https://doi.org/10.1016/J.MATTOD.2020.09.004.

[14] Y. Li, M. Gu, M. Zhang, X. Zhang, K. Lv, Y. Liu, W. Ho, F. Dong, C_3N_4 with engineered three coordinated ($N3_C$) nitrogen vacancy boosts the production of $^1O_2$ for Efficient and stable NO photo-oxidation, Chem. Eng. J. 389 (2020) 124421, https://doi.org/10.1016/j.cej.2020.124421.

[15] L.i. Zhou, H. Zhang, H. Sun, S. Liu, M.O. Tade, S. Wang, W. Jin, Recent advances in non-metal modification of graphitic carbon nitride for photocatalysis: a historic review, Catal, Sci. Technol. 6 (19) (2016) 7002–7023, https://doi.org/10.1039/C6CY01195K.

[16] V. Hasija, P. Raizada, A. Sudhaik, K. Sharma, A. Kumar, P. Singh, S. B. Jonnalagadda, V.K. Thakur, Recent advances in noble metal free doped graphitic carbon nitride based nanohybrids for photocatalysis of organic contaminants in water: A review, Appl. Mater. Today. 15 (2019) 494–524, https://doi.org/10.1016/J.APMT.2019.04.003.

[17] H. Starukh, P. Praus, Doping of Graphitic Carbon Nitride with Non-Metal Elements and Its Applications in Photocatalysis, Catal. 2020, Vol. 10, Page 1119. 10 (2020) 1119. doi:10.3390/CATAL10101119.

[18] W.-J. Ong, L.-L. Tan, Y.H. Ng, S.-T. Yong, S.-P. Chai, Graphitic Carbon Nitride (g-C3N4)-Based Photocatalysts for Artificial Photosynthesis and Environmental Remediation: Are We a Step Closer to Achieving Sustainability? Chem. Rev. 116 (12) (2016) 7159–7329.

[19] R. Kavitha, P.M. Nithya, S. Girish Kumar, Noble metal deposited graphitic carbon nitride based heterojunction photocatalysts, Appl. Surf. Sci. 508 (2020) 145142, https://doi.org/10.1016/j.apsusc.2019.145142.

[20] X. Li, Z. Hu, Q. Li, M. Lei, J. Fan, S.A.C. Carabineiro, Y.i. Liu, K. Lv, Three in one: atomically dispersed Na boosting the photoreactivity of carbon nitride towards NO oxidation, Chem. Commun. 56 (91) (2020) 14195–14198, https://doi.org/10.1039/D0CC05948J.

[21] C. Yang, Q. Tan, Q. Li, J. Zhou, J. Fan, B. Li, J. Sun, K. Lv, 2D/2D Ti_3C_2 MXene/g-C_3N_4 nanosheets heterojunction for high efficient CO_2 reduction photocatalyst: Dual effects of urea, Appl. Catal. B Environ. 268 (2020) 118738, https://doi.org/10.1016/j.apcatb.2020.118738.

[22] V. Muelas-Ramos, M.J. Sampaio, C.G. Silva, J. Bedia, J.J. Rodriguez, J.L. Faria, C. Belver, Degradation of diclofenac in water under LED irradiation using combined g-C_3N_4/NH_2-MIL-125 photocatalysts, J. Hazard. Mater. 416 (2021) 126199, https://doi.org/10.1016/j.jhazmat.2021.126199.

[23] S.N. Guo, Y. Zhu, Y.Y. Yan, Y.L. Min, J.C. Fan, Q.J. Xu, Holey structured graphitic carbon nitride thin sheets with edge oxygen doping via photo-Fenton reaction with enhanced photocatalytic activity, Appl. Catal. B Environ. 185 (2016) 315–321, https://doi.org/10.1016/J.APCATB.2015.11.030.

[24] D. Zhao, C.-L. Dong, B. Wang, C. Chen, Y.-C. Huang, Z. Diao, S. Li, L. Guo, S. Shen, D. Zhao, B. Wang, Z. Diao, L. Guo, S. Shen, C. Dong, Y. Huang, C. Chen, S. Li,

Synergy of Dopants and Defects in Graphitic Carbon Nitride with Exceptionally Modulated Band Structures for Efficient Photocatalytic Oxygen Evolution, Adv. Mater. 31 (2019) 1903545, https://doi.org/10.1002/ADMA.201903545.
[25] Y. Wen, D. Qu, L.i. An, X. Gao, W. Jiang, D. Wu, D. Yang, Z. Sun, Defective g-C_3N_4 Prepared by the $NaBH_4$ Reduction for High-Performance H_2 Production, ACS Sustain. Chem. Eng. 7 (2) (2019) 2343–2349.
[26] H. Xu, Z. Wu, Y. Wang, C. Lin, Enhanced visible-light photocatalytic activity from graphene-like boron nitride anchored on graphitic carbon nitride sheets, J. Mater. Sci. 52 (16) (2017) 9477–9490.
[27] U. Caudillo-Flores, D. Rodríguez-Padrón, M.J. Muñoz-Batista, A. Kubacka, R. Luque, M. Fernández-García, Facile synthesis of B/g-C_3N_4 composite materials for the continuous-flow selective photo-production of acetone, Green Chem. 22 (15) (2020) 4975–4984, https://doi.org/10.1039/D0GC01326A.
[28] Y.-P. Zhu, T.-Z. Ren, Z.-Y. Yuan, Mesoporous Phosphorus-Doped g-C_3N_4 Nanostructured Flowers with Superior Photocatalytic Hydrogen Evolution Performance, ACS Appl. Mater. Interfaces. 7 (30) (2015) 16850–16856.
[29] K. Wang, Q. Li, B. Liu, B. Cheng, W. Ho, J. Yu, Sulfur-doped g-C_3N_4 with enhanced photocatalytic CO_2-reduction performance, Appl. Catal. B Environ. 176–177 (2015) 44–52, https://doi.org/10.1016/J.APCATB.2015.03.045.
[30] G. Zhang, M. Zhang, X. Ye, X. Qiu, S. Lin, X. Wang, G. Zhang, M. Zhang, X. Ye, X. Qiu, S. Lin, X. Wang, Iodine Modified Carbon Nitride Semiconductors as Visible Light Photocatalysts for Hydrogen Evolution, Adv. Mater. 26 (2014) 805–809, https://doi.org/10.1002/ADMA.201303611.
[31] Y. Wang, Y. Di, M. Antonietti, H. Li, X. Chen, X. Wang, Excellent visible-light photocatalysis of fluorinated polymeric carbon nitride solids, Chem. Mater. 22 (18) (2010) 5119–5121.
[32] C.N.R. Rao, K. Gopalakrishnan, Borocarbonitrides, $B_xC_yN_z$: Synthesis, Characterization, and Properties with Potential Applications, ACS Appl. Mater. Interfaces. 9 (23) (2017) 19478–19494.
[33] R. Bahadur, G. Singh, Y. Bando, A. Vinu, Advanced porous borocarbonitride nanoarchitectonics: Their structural designs and applications, Carbon N. Y. 190 (2022) 142–169, https://doi.org/10.1016/J.CARBON.2022.01.013.
[34] D. Mateo, J.L. Cerrillo, S. Durini, J. Gascon, Fundamentals and applications of photo-thermal catalysis, Chem. Soc. Rev. 50 (3) (2021) 2173–2210, https://doi.org/10.1039/D0CS00357C.
[35] S. Najafishirtari, K. Friedel Ortega, M. Douthwaite, S. Pattisson, G.J. Hutchings, C. J. Bondue, K. Tschulik, D. Waffel, B. Peng, M. Deitermann, G.W. Busser, M. Muhler, M. Behrens, A Perspective on Heterogeneous Catalysts for the Selective Oxidation of Alcohols, Chem. – A Eur. J. 27 (68) (2021) 16809–16833.
[36] X. Zhao, Q. Liu, Q. Li, L. Chen, L. Mao, H. Wang, S. Chen, Two-dimensional electrocatalysts for alcohol oxidation: A critical review, Chem. Eng. J. 400 (2020) 125744, https://doi.org/10.1016/j.cej.2020.125744.
[37] V. Nair, M.J. Muñoz-Batista, M. Fernández-García, R. Luque, J.C. Colmenares, Thermo-Photocatalysis: Environmental and Energy Applications, ChemSusChem. 12 (10) (2019) 2098–2116.
[38] P. Makuła, M. Pacia, W. Macyk, How to correctly determine the band gap energy of modified semiconductor photocatalysts based on UV-vis spectra, J. Phys. Chem. Lett. 9 (23) (2018) 6814–6817, https://doi.org/10.1021/acs.jpclett.8b02892.
[39] H.A. Duarte, P.J. Luggren, J. Zelin, M.E. Sad, V.K. Díez, J.I. Di Cosimo, Selective aerobic oxidation of benzyl alcohol on inexpensive and reusable ZnO/$MnCO_3$ catalyst, Catal. Today. 394-396 (2022) 178–189.
[40] J. Lee, J. Kim, W. Choi, Ferrioxalate-Polyoxometalate System as a New Chemical Actinometer, Environ. Sci. Technol. 41 (15) (2007) 5433–5438.
[41] J.N. Miller, J.C. Miller, R.D. Miller, Statistics and chemometrics for analytical chemistry, Seventh ed, Pearson Education Limited, Harlow (United Kingdom), 2018.
[42] N. Serpone, Relative photonic efficiencies and quantum yields in heterogeneous photocatalysis, J. Photochem. Photobiol. A Chem. 104 (1-3) (1997) 1–12, https://doi.org/10.1016/S1010-6030(96)04538-8.
[43] G. Li Puma, A. Brucato, Dimensionless analysis of slurry photocatalytic reactors using two-flux and six-flux radiation absorption–scattering models, Catal. Today. 122 (1-2) (2007) 78–90.
[44] O.M. Alfano, D. Bahnemann, A.E. Cassano, R. Dillert, R. Goslich, Photocatalysis in water environments using artificial and solar light, Catal. Today. 58 (2-3) (2000) 199–230, https://doi.org/10.1016/S0920-5861(00)00252-2.
[45] M.J. Muñoz-Batista, A. Kubacka, O. Fontelles-Carceller, D. Tudela, M. Fernández-García, Surface CuO, Bi_2O_3, and CeO_2 Species Supported in TiO_2-Anatase: Study of Interface Effects in Toluene Photodegradation Quantum Efficiency, ACS Appl. Mater. Interfaces. 8 (22) (2016) 13934–13945.
[46] M. Kim, S. Hwang, J.-S. Yu, Novel ordered nanoporous graphitic C_3N_4 as a support for Pt–Ru anode catalyst in direct methanol fuel cell, J. Mater. Chem. 17 (17) (2007) 1656–1659, https://doi.org/10.1039/B702213A.
[47] S. Sunasee, K.H. Leong, K.T. Wong, G. Lee, S. Pichiah, InWook Nah, B.-H. Jeon, Y. Yoon, M. Jang, Sonophotocatalytic degradation of bisphenol A and its intermediates with graphitic carbon nitride, Environ. Sci. Pollut. Res. 26 (2) (2019) 1082–1093.
[48] X. Wang, B. Liu, X. Xiao, S. Wang, W. Huang, Boron dopant simultaneously achieving nanostructure control and electronic structure tuning of graphitic carbon nitride with enhanced photocatalytic activity, J. Mater. Chem. C. 9 (41) (2021) 14876–14884, https://doi.org/10.1039/D1TC04142H.
[49] X. She, J. Wu, J. Zhong, H. Xu, Y. Yang, R. Vajtai, J. Lou, Y. Liu, D. Du, H. Li, P. M. Ajayan, Oxygenated monolayer carbon nitride for excellent photocatalytic hydrogen evolution and external quantum efficiency, Nano Energy. 27 (2016) 138–146, https://doi.org/10.1016/J.NANOEN.2016.06.042.
[50] M.O. Watanabe, S. Itoh, K. Mizushima, T. Sasaki, Bonding characterization of BC_2N thin films, Appl. Phys. Lett. 68 (21) (1996) 2962–2964, https://doi.org/10.1063/1.116369.
[51] M. Dinescu, A. Perrone, A.P. Caricato, L. Mirenghi, C. Gerardi, C. Ghica, L. Frunza, Boron carbon nitride films deposited by sequential pulses laser deposition, Appl. Surf. Sci. 127–129 (1998) 692–696, https://doi.org/10.1016/S0169-4332(97)00727-7.
[52] M.J. Lima, P.B. Tavares, A.M.T. Silva, C.G. Silva, J.L. Faria, Selective photocatalytic oxidation of benzyl alcohol to benzaldehyde by using metal-loaded g-C_3N_4 photocatalysts, Catal. Today. 287 (2017) 70–77, https://doi.org/10.1016/J.CATTOD.2016.11.023.
[53] M.J. Lima, A.M.T. Silva, C.G. Silva, J.L. Faria, Graphitic carbon nitride modified by thermal, chemical and mechanical processes as metal-free photocatalyst for the selective synthesis of benzaldehyde from benzyl alcohol, J. Catal. 353 (2017) 44–53, https://doi.org/10.1016/J.JCAT.2017.06.030.
[54] S. Samanta, S. Khilari, D. Pradhan, R. Srivastava, An efficient, visible light driven, selective oxidation of aromatic alcohols and amines with O_2 using $BiVO_4$/g-C_3N_4 nanocomposite: a systematic and comprehensive study toward the development of a photocatalytic p, ACS Sustain. Chem. Eng. 5 (2017) 2562–2577, https://doi.org/10.1021/ACSSUSCHEMENG.6B02902.
[55] A. Magdziarz, J.C. Colmenares, O. Chernyayeva, D. Lisovytskiy, J. Grzonka, K. Kurzydłowski, K. Freindl, J. Korecki, Insight into the synthesis procedure of Fe^{3+}/TiO_2-based photocatalyst applied in the selective photo-oxidation of benzyl alcohol under sun-imitating lamp, Ultrason. Sonochem. 38 (2017) 189–196, https://doi.org/10.1016/J.ULTSONCH.2017.03.012.
[56] J. Tripathy, G. Loget, M. Altomare, P. Schmuki, Polydopamine-coated TiO2 nanotubes for selective photocatalytic oxidation of benzyl alcohol to benzaldehyde under visible light, J. Nanosci. Nanotechnol. 16 (2016) 5353–5358, https://doi.org/10.1166/JNN.2016.12595.
[57] M. Pelaez, P. Falaras, V. Likodimos, K. O'Shea, A.A. de la Cruz, P.S.M. Dunlop, J. A. Byrne, D.D. Dionysiou, Use of selected scavengers for the determination of NF-TiO_2 reactive oxygen species during the degradation of microcystin-LR under visible light irradiation, J. Mol. Catal. A Chem. 425 (2016) 183–189, https://doi.org/10.1016/j.molcata.2016.09.035.
[58] J.T. Schneider, D.S. Firak, R.R. Ribeiro, P. Peralta-Zamora, Use of scavenger agents in heterogeneous photocatalysis: truths, half-truths, and misinterpretations, Phys. Chem. Chem. Phys. 22 (27) (2020) 15723–15733.
[59] R. Palominos, J. Freer, M.A. Mondaca, H.D. Mansilla, Evidence for hole participation during the photocatalytic oxidation of the antibiotic flumequine, J. Photochem. Photobiol. A Chem. 193 (2-3) (2008) 139–145.